DFT Study on the Electronic Properties, Spectroscopic Profile, and Biological Activity of 2-Amino-5-trifluoromethyl-1,3,4-thiadiazole with Anticancer Properties

Isha Singh, Lamya H. Al-Wahaibi,* Ruchi Srivastava, Onkar Prasad, Shilendra K. Pathak, Saurabh Kumar, Shama Parveen, Monisha Banerjee, Ali A. El-Emam, and Leena Sinha*
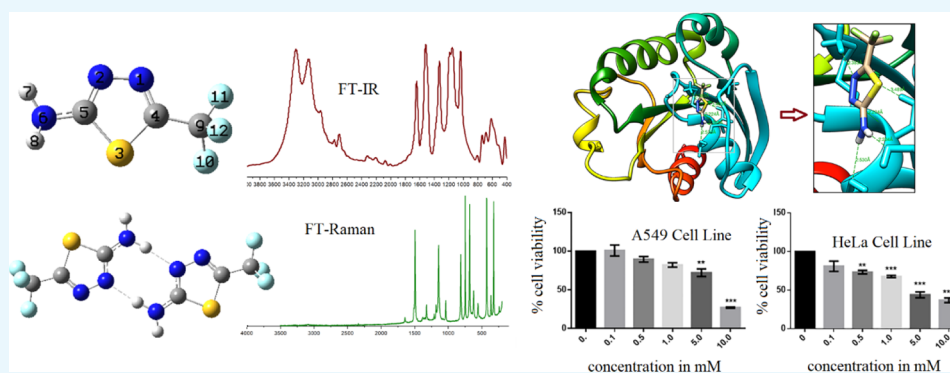
Read Online

ACCESS | Metrics & More | Article Recommendations | SI Supporting Information

ABSTRACT: Extensive investigation on the molecular and electronic structure of 2-amino-5-trifluoromethyl-1,3,4-thiadiazole in the ground state and in the first excited state has been performed. The energy barrier corresponding to the conversion between imino and amino tautomers has been calculated, which indicates the existence of amino tautomer in solid state for the title compound. The FT−Raman and FT-IR spectra were recorded and compared with theoretical vibrational wavenumbers, and a good coherence has been observed. The MESP map, dipole moment, polarizability, and hyperpolarizability have been calculated to comprehend the properties of the title molecule. High polarizability value estimation of the title compound may enhance its bioactivity. Natural bonding orbital analysis has been done on monomer and dimer to investigate the charge delocalization and strength of hydrogen bonding, respectively. Strong hydrogen bonding interaction energies of 17.09/17.49 kcal mol^{-1} have been calculated at the B3LYP/M06-2X functional. The UV−vis spectrum was recorded and related to the theoretical spectrum. The title compound was biologically examined for anticancer activity by studying the cytotoxic performance against two human cancer cell lines (A549 and HeLa) along with the molecular docking simulation. Both molecular docking and cytotoxic performance against cancer cell lines show positive outcomes, and the title compound appears to be a promising anticancer agent.

1. INTRODUCTION

Heterocyclic compounds consisting of fluorine, in general, are of copious interest in recent medicinal chemistry. The structural moiety of the trifluoromethyl group (CF_3) has various classes of bioactive organic molecules, which exhibit a wide range of biological properties.[1,2] It has been reported that the CF_3-substituted compounds possess biological activities such as anticancer and antipyretic and are used as analgesic agents, herbicides, and fungicides.[3,4] Because fluorine is the most electronegative halogen atom in nature, it has a major effect on the electron distribution, basicity, or acidity of adjoining groups and can alter the reactivity as well as the stability of the molecule.[5] The expedient induction of fluorine into a molecule can adequately influence their intrinsic potency, metabolic pathways, membrane permeability, and pharmacokinetic properties.[6,7]

Romano *et al.*[8] have reported the computational studies of 5-difluoromethyl-1,3,4-thiadiazole-2-amino (DFTA), a difluoro-substituted compound of 2-amino-5-methyl-1,3,4-thiadiazole. The derivatives of 2-amino-5-methyl-1,3,4-thiadiazole are vital from the pharmacological point of view as they exhibit a wide spectrum of anticancer activities,[9−15] while 2-amino-1,3,4-thiadiazole itself can be used for the treatment of leukemia L1210 cells by reducing adenine and guanine ribonucleotide

pools.[16] The parent compound 1,3,4-thiadiazole itself forms an important class of intermediates in the medical field, pesticides, polymer chemistry, and chemical synthesis. Both symmetrical and asymmetrical 1,3,4-thiadiazoles have been reported to exhibit important biological activities such as antitumor,[17] anticancer,[18−20] antibacterial,[21] antifungal,[22] antimicrobial,[23,24] antituberculosis,[25] anti-inflammatory,[26,27] antihypertensive,[28,29] anticonvulsant,[30,31] antioxidant,[32] anesthetic,[33,34] and cardiotonic.[35]

In the present work, we have performed combined theoretical computational and experimental studies on 2-amino-5-trifluoromethyl-1,3,4-thiadiazole (ATFT), a trifluoromethyl-substituted compound of 2-amino-5-methyl-1,3,4-thiadiazole, with the hope that the present investigation may initiate the usage of the title compound for several medical purposes. We have also compared the reactivity descriptors of the title compound with those of DFTA to gauge the effect of an additional fluorine atom. In addition to the comprehensive study on the molecular structure, spectroscopic imprint, and electronic properties, the compound ATFT has also been biologically examined for its anticancer activity by studying the cytotoxic performance against two human cancer cell lines and along with the molecular docking simulation. To the best of our knowledge, no such theoretical study has been reported related to its geometry and assignments of vibrational spectra. The UV spectrum for the title compound has also been simulated and compared with the experimental results in various solutions. The transition wavelengths calculated by TD-DFT results are in good agreement with the experimental data. As the monomer of the title compound joins to form dimers by N−H···N hydrogen bonds, we have performed natural bonding orbital (NBO) analysis of monomer as well as dimer to estimate the strength of the hydrogen bond and to assess the charge transfer (inter- and intramolecular) within the system. The theory of atoms in molecules by Bader[36] has also been used to calculate the intermolecular hydrogen bond strength. The thermodynamical and nonlinear optical properties along with the 3D molecular electrostatic potential surface (MESP) have been studied using the tools of quantum chemistry.

2. COMPUTATIONAL DETAILS

In order to obtain comprehensive information related to the structural features and properties of the title compound, gradient-corrected DFT[37] with Becke's 3 exchange[38] Lee−Yang−Parr correlation functional (B3LYP)[39] and M06-2X[40] functional methods with the basis set 6-311++G(d,p) has been employed. B3LYP is the most popular DFT functional and widely used in density functional calculations.[41] It is a satisfactory and reliable choice between accuracy and computational cost for medium size molecules, but problems arise as the size of the system increases—imprecise calculation of heat of formation,[42] reaction barrier heights are underestimated,[43] failure in the correct portrayal of van der Waals interactions,[44] and unreliable energy ordering of isomers are some drawbacks. Truhlar's M06 family of functionals[45] performs reasonably for nonbonded interactions, greatly increasing the applicability of DFT methods. The M06-2X hybrid with greater exact exchange than B3LYP performs far better than B3LYP for a dispersive and hydrogen bonding system. The B3LYP functional extended with the triple-zeta 6-311++G(d,p) (polarized) basis set used in the present study provides an overall decent description of small- and medium-sized molecules, while M06-2X[40] is a global hybrid functional and is the top performer within the M06 functional family for noncovalent interactions, thermochemistry, and kinetics. All calculations related to this study have been executed with the computational chemistry software package Gaussian 09 program[46] and results were analyzed with the help of the GaussView 5.0 program,[47] which has a graphical interface with Gaussian for molecular visualization.

The molecular properties such as ground-state energy, frontier orbital energies, dipole moment, polarizability, and hyperpolarizability have been studied using both B3LYP and M06-2X functionals. The vibrational wavenumbers under harmonic estimation were determined at the same level of theory, and the absence of non-negative values of vibrational wavenumbers established the stability of the structure corresponding to a true minimum on potential energy surface. The optimized geometry of the title molecule and its hydrogen-bonded dimer is presented in Figure 1, whereas
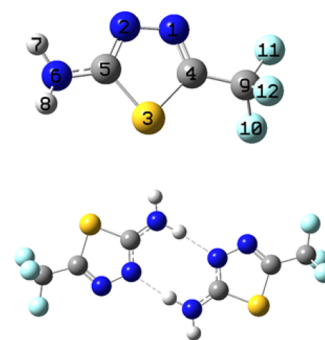

Figure 1. Optimized structure of ATFT and its hydrogen-bonded dimer at DFT/B3LYP/6-311++G(d,p).

the geometrical parameters calculated at DFT/B3LYP and DFT/M06-2X with 6-311++G(d,p) basis set are reported in Table 1. The optimized parameters of ATFT are very close to the experimental values of the same as reported by Boechat *et al.*[48]

To omit the systematic errors brought by basis set inadequacy and vibrational anharmonicity,[49] reasonable uniform scaling variables of 0.983 up to 1700 cm⁻¹ and 0.958 for larger than 1700 cm⁻¹[50,51] have been used for B3LYP and a constant scaling factor of 0.9489[52,53] has been used for M06-2X. The MOLVIB program (V7.0-G77) by Sundius[54−56] has been utilized to compute percentage potential energy distribution (PED) and hence to correctly assign the vibrational wavenumbers of the title compound.

The theoretical UV−vis spectrum is computed by the TD-DFT method for the gas phase, and the integral equation formalism polarizable continuum model (IEFPCM) has been used for investigating the effect of solvents on electron excitation. The electronic properties such as frontier molecular orbital (MO) LUMO and HOMO energies and their band gaps have also been determined by the TD-DFT method. NBOs[57] have maximum electron density and help us to estimate the intramolecular delocalization/hyperconjugation as well as to make out different second-order interactions between the filled Lewis orbitals (occupancy = 2) of one segment and empty non-Lewis orbitals (occupancy = 0) of another segment of the molecular system. As a result of donor−acceptor interactions, there is a loss of occupancy from the NBO with an ideal Lewis structure into an empty non-

Table 1. Optimized geometric parameters for ATFT at B3LYP and M06-2X along with the corresponding experimental data

bond length	exp. (Å)	cal. value (Å)		bond angle	cal. value (deg)	
		B3LYP	M06-2X		B3LYP	M06-2X
N1−N2	1.378	1.358	1.356	S3−C4−C9	122.2	122.0
N2−C5	1.328	1.309	1.301	N1−C4−C9	123.4	123.1
N1−C4	1.291	1.289	1.283	F11−C9−C4	111.9	111.7
C4−S3	1.727	1.760	1.742	F10−C9−C4	110.8	110.5
S3−C5	1.749	1.759	1.745	F12−C9−C4	111.3	111.1
C5−N6	1.325	1.363	1.364	F12−C9−F11	107.9	108.1
C4−C9	1.494	1.011	1.011	F10−C9−F11	108.2	108.5
C9−F10	1.324	1.007	1.008	F10−C9−F12	106.5	106.8
C9−F12	1.331	1.503	1.502		cal. value (deg)	
C9−F11	1.312	1.355	1.342	dihedral angle	B3LYP	M06-2X
		1.355	1.340	F11−C9−C4−S3	165.1	163.4
		1.333	1.323	F10−C9−C4−N1	139.1	140.9
		cal. value (deg)		F12−C9−C4−N1	102.7	100.8
bond angle	exp. value (deg)	B3LYP	M06-2X	C9−C4−S3−C5	176.6	176.3
H8−N6−H7		115.6	115.0	N1−C4−S3−C5	0.5	0.5
C5−N6−H7		114.7	113.6	C4−S3−C5−N2	0.4	0.5
C5−N6−H8		119.0	118.1	C4−S3−C5−N6	176.6	176.4
S3−C5−N6	122.35	122.5	122.2	C9−C4−N1−N2	176.6	176.4
N2−C5−N6	124.1	123.2	123.2	S3−C4−N1−N2	0.4	0.5
S3−C5−N2	113.56	114.2	114.4	C4−N1−N2−C5	0.1	0.0
C5−N2−N1	111.81	112.6	112.4	N1−N2−C5−S3	0.3	0.4
C5−S3−C4	86.3	85.1	85.1	N1−N2−C5−N6	176.5	176.3
S3−C4−N1	115.29	114.4	114.9	S3−C5−N6−H8	29.2	32.8
C4−N1−N2	113.03	113.7	113.2	N2−C5−N6−H7	12.1	12.5

Lewis NBO. The stabilization energy $E_{(2)}$ related to the delocalization i (donor) → j (acceptor) is estimated as

$$E_{(2)} = \Delta E_{ij} = q_i \frac{F(i,j)^2}{\varepsilon_i - \varepsilon_j}$$

where q_i is the donor orbital occupancy, ε_i and ε_j are the diagonal elements, and $F(i,j)$ is the off-diagonal NBO Fock matrix element. These calculations help us to investigate the probable charge transfer within the molecule and the intermolecular bond paths.

The total Raman intensities were calculated from the Raman activities (S_i) obtained from the Gaussian 09W program utilizing the following relationship obtained from the intensity theory of Raman scattering[58,59]

$$I_i = [f(\nu_o - \nu_i)^4 S_i]/[\nu_i\{1 - \exp(-hc\nu_i/kT)\}]$$

where ν_o is the wavenumber in cm^{-1} of the exciting light; ν_i is the vibrational wavenumber of the ith mode; h, c, and k are the fundamental constants; and f is a reasonably picked standardization factor for all peak intensities. The theoretical IR and Raman spectra have been plotted utilizing the undulated Lorentzian band shape with a full width at half-maximum of 10 cm^{-1}. Based on vibrational wavenumber calculations at different temperatures, the thermodynamic properties of the title compound have also been computed and fitted by quadratic formulae.

All computations related to docking were performed on Auto Dock/Vina software,[60] which applies the Lamarckian genetic algorithm (LGA).[61] The 3D crystal structure of the protein in PDB format was obtained from the RCSB Protein Data Bank. As required in the LGA, for selected chain A of the protein, all water molecules were removed and the polar hydrogen atoms were added, followed by the calculation of

Kollman and Gasteiger charges. After docking, all the docked conformations were viewed using a Discovery Studio Visualizer[62] for bonding interactions and chimera[63] for hydrogen bonds.

3. RESULTS AND DISCUSSION

3.1. Geometry Optimization. The crystallographic data of the title compound[48] show that it crystallizes in a space group, $P2_1/c$. The crystal belongs to a monoclinic system with the following lattice parameters: a = 9.1082 Å, b = 6.9373 Å, c = 10.8048 Å, β = 116.656°, and its unit cell volume being 610.15 Å^3. The ground-state energy of the title molecule is calculated to be at −977.66671 and −977.43856 Hartree at the B3LYP and M06-2X functionals, respectively. The optimized geometrical parameters, such as bond lengths, bond angles, and dihedral angles, are collected in Table 1, and it was found that the calculated parameters at both the functionals are in good concurrence with the experimental ones. All the dihedral angles of the 1,3,4-thiadiazole ring are nearly 0°, which demonstrates its planar nature. The dihedral angles (C4−S3−C5−N6 and N1−N2−C5−N6) illustrating the orientation of the 1,3,4-thiadiazole ring with respect to the nitrogen atom of the amino group are around 176.5°.

According to the crystal structure, the molecules are linked into centrosymmetric R_2^2 (8) dimers by paired N−H⋯N hydrogen bonds;[48] thus, it is interesting to calculate the rotational barrier of nitrogen of the amino group with a carbon of the thiadiazole ring. For analysis of the transition state of the title compound to calculate the rotational barrier, frequency calculations have also been done at the DFT-B3LYP/6-311+ +G(d,p) level of theory. The rotational barrier (ΔE_{rot}) is computed as the electronic energy difference between the transition state (single negative frequency) and its corresponding minima. For the title compound, this rotational barrier of

Table 2. Dipole Moment, Energies of Important MOs in eV, and Their Energy Gap for ATFT

parameters	TD-DFT/B3LYP/6-311++G(d,p)		
	gas	methanol	water
E_{total} (Hartree)	−977.66671	−977.67962	−977.68004
E_{total} (eV)	−26603.67441	−26604.02571	−26604.03714
E_{LUMO+1}	−1.20901	−0.7943	−0.78314
E_{LUMO}	−1.82153	−1.73364	−1.73228
E_{HOMO}	−7.34327	−7.14136	−7.13646
E_{HOMO-1}	−8.01103	−8.11417	−8.11961
$\Delta E_{(HOMO)-(LUMO)}$	5.52174	5.40772	5.40418
$\Delta E_{(HOMO-1)-(LUMO)}$	6.18950	6.38053	6.38733
$\Delta E_{(HOMO)-(LUMO+1)}$	6.13427	6.34706	6.35332
$\Delta E_{(HOMO-1)-(LUMO+1)}$	6.80203	7.31987	7.33646
	Dipole Moment (debey)		
μ_x	−4.4625	−5.4496	−5.4760
μ_y	−3.0746	−4.3526	−4.4016
μ_z	0.7343	0.9127	0.9202
μ_{tot}	5.4687	7.0340	7.0857

the NH_2 group is calculated to be 6.08057 kcal/mol. Figure S1a shows the rotation process, transition state, and energy barrier associated with the rotation process.

Romano et al.[8] have studied the interconversion of amine and imine tautomers for DFTA, and the energy difference at B3LYP/6-311++G(d,p) is calculated to be 4.45029 kcal/mol. They have reported the coexistence of both amino and imine tautomers due to the small energy difference between the two. Their theoretical IR assignments of normal modes of vibrations correspond to the average for amine and imine tautomers. In light of the work reported by Romano et al.,[8] it is essential to calculate the reaction path for the conversion of amine to imine tautomer for the title compound. The reaction path for the conversion of amine to imine tautomer along with the transition state is computed for the title compound and found to be 44.47788 kcal/mol [Figure S1b], which is quite higher as compared to that of DFTA as reported by Romano et al.[8] This shows the role of the third fluorine atom in preventing the interconversion of amine and imine and hence indicating the existence of amine tautomer in solid state for the title compound. The data presented in this study henceforth corresponds to amino tautomer unless otherwise stated.

The 1,3,4-thiadiazole N−N bond length is calculated to be 1.358 Å for the B3LYP functional. The C5−N6 bond length joining the thiadiazole ring to the amino group is calculated to be at 1.363 Å (1.364 Å) at B3LYP (M06-2X) because of the partial double bond characteristic, which is very much different from the value at 1.491 Å, as calculated for DFTA, which clearly indicates the effect of the third fluorine atom in the title compound as compared to DFTA. The bond lengths of N6−H8 (1.007 Å) and N6−H7 (1.011 Å) are in good agreement as reported by Romano et al.[8] for DFTA. The optimized bond lengths of C9−F12 and C9−F10 are found at 1.355 Å at B3LYP and 1.340 and 1.342 Å, respectively, at M06-2X. The values of bond angles N2−C5−N6 and C5−S3−C4 are found to be the same at 123.2 and 85.1° for both the functionals and are also in very good agreement with the experimental values at 124.1 and 86.3°. The bond angles C5−N6−H8 and S3−C4−N1 are calculated at 119.0 and 114.4°, respectively, for B3LYP, and they are nearly the same for M06-2X at 118.1 and 114.9°, respectively. Because we analyzed that all the determined geometrical parameters of the optimized molecular structure of the title compound are close to their experimental quantities, it

may be utilized to find different molecular and spectroscopic parameters.

3.2. Electronic Properties and UV−Vis Studies. The HOMO−LUMO band gap is a basic parameter in deciding atomic electrical transport properties such as the chemical reactivity of a substance and kinetic stability of a molecule because it is a measure of electron conductivity.[64] The optimized ground-state structure has been utilized to determine the excited states of the title compound at the B3LYP and M06-2X functionals. The energies and 3D plots of HOMO (MO 42), LUMO (MO 43), and other MOs engaged in the UV transitions for the title compound are given in Table 2 and Figure 2 at B3LYP/TD-DFT/6-311++G(d,p).

The electronic transitions calculated using the M06-2X functional are also given in Table 3. The HOMO as well as the LUMO of the title compound is distributed over the entire molecule with LUMO having more antibonding characteristic. The calculated energy gap is 5.52174 eV, which is smaller than the energy gap for DFTA (ΔE = 5.5397 eV) and 1,3,4-thiadiazole (ΔE = 6.15767 eV), implying that the presence of the CF_3 group in ATFT increases its reactivity. As the tautomeric equilibrium is predominantly affected by the nature of the solvent and protic solvents such as water and methanol can shift the equilibrium toward imine tautomer, it is important to check the possibility of the existence of imine tautomer in water and methanol, and hence, we have calculated the theoretical UV spectrum for amine as well as imine tautomer. The experimentally measured and theoretically calculated UV−vis spectra in methanol and water for the title compound (imine and amine tautomer) are shown in Figure 3. Absorption wavelengths (λ) corresponding to electronic transition, oscillator strengths (f), and vertical excitation energies (E) along with the experimental values are exhibited in Table 3. The absorption maxima for amine tautomer are calculated at 254.95 nm in methanol and at 255.11 nm in water, which is due to an electronic transition from HOMO (MO-42) to the LUMO (MO-43). This transition for imine tautomer shifts to 268 nm in water, which is in between the experimental peaks at 254 and 291 nm, which indicates the possible existence of imine tautomer in the solution.

3.3. Molecular Electrostatic Potential Surface and Global Reactivity Descriptors. A plot of molecular
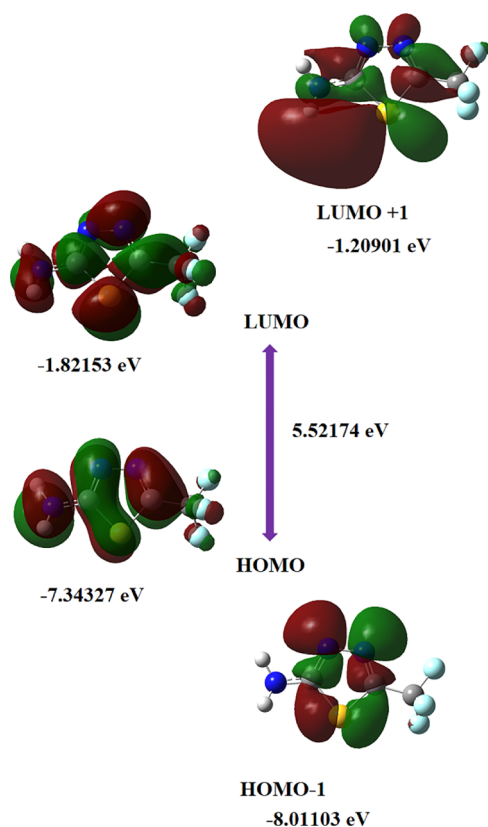
Figure 2. Patterns of the HOMO, LUMO, and other significant MOs of ATFT.

electrostatic potential surface (MESP) with a color-coding scheme to represent the electrophilic and nucleophilic sites in a molecule is a very effective method and extremely advantageous to examine the correlation between the molecular structure and the physicochemical property relationship in biomolecules. The red region shows the electron-rich region and the blue region shows the electron-poor area, while the green region refers to the neutral region. The MESP map of the title compound shown in Figure S2 clearly suggests that the electropositive potential region (blue shade) is around an amino group of the title compound and the electronegative

region is found around the nitrogen atom of the thiadiazole ring, whereas the rest of the compound appears to have practically neutral electrostatic potential.

The descriptors which are helpful in analyzing the global reactivity of the molecule such as electronegativity, hardness, softness, and electrophilicity index can be calculated using ionization potential (I) and electron affinity (A). The ionization potential and electron affinity can be calculated as the difference between the ground-state energy of the cationic and neutral system and the difference between the ground-state energy of the neutral and anionic system, respectively, that is, $I = E(N − 1) − E(N)$ and $A = E(N) − E(N + 1)$. Electronegativity (χ) is the negative chemical potential, and electronic chemical potential as introduced by Parr and Pearson[65] is calculated as $\mu_{cp} = −(I + A)/2$, which describes the proclivity of electrons to leave a stable system, while chemical hardness "η" given by $(I − A)/2$ is a parameter to measure the resistance to alter the electron distribution and hence can be associated with the reactivity of the chemical system. Following Parr and Yang,[66] the global electrophilicity index (ω) is calculated with the help of chemical potential (μ_{cp}) and chemical hardness (η) using the formula $\omega = \mu_{cp}^2/2\eta$. A comparative study of global reactivity descriptors has been done for the title molecule, DFTA, and 1,3,4-thiadiazole. The comparative table (Table 4) of the reactivity descriptors clearly reflects that the title molecule is more chemically reactive (less hard and softer) than 1,3,4-thiadiazole and DFTA.

The work reported by Domingo et al.[67] classifies the organic molecules on the basis of electrophilicity index ω as marginal electrophiles with $\omega < 0.8$ eV, moderate electrophiles with $0.8 < \omega < 1.5$ eV, and strong electrophiles having $\omega > 1.5$ eV. The title compound with $\omega = 2.57342$ eV will behave as a strong electrophile and $\mu = −4.71160$ eV also indicates the electron-withdrawing characteristic.[67]

3.4. Electric Moments. For the idea of the nonlinear optical activities of the title compound, electric moments, for example, dipole moment, polarizability, and first-order hyperpolarizability have been calculated at the same level of theory using the B3LYP and M06-2X functionals. The title compound possesses a high dipole moment value estimated at 5.4687 debye in the gas phase, which increases sharply to 7.0340

Table 3. Experimental and Calculated Absorption Wavelength λ (nm) and Excitation Energies E (eV) of ATFT

| experimental		TD-DFT/B3LYP/6-311++G(d,p) monomer			TD-DFT/B3LYP/6-311++G(d,p) dimer			TD-DFT/M06-2X/6-311++G(d,p) monomer		
λ (nm)	E (eV)	λ (nm)	E (eV)	f	λ (nm)	E (eV)	f	λ (nm)	E (eV)	f
					Methanol					
254.62	4.8694	254.95 (42−43)	4.8632	0.1913	266.47	4.6528	0.0000	233.05 (42−43)	5.3201	0.1505
291.49	4.2535	244.40 (41−43)	5.0730	0.0083	264.28	4.6914	0.2238	228.46 (41−43)	5.4269	0.0737
		239.00 (42−44)	5.1876	0.0034	257.19	4.8208	0.2215	219.83 (42−45)	5.6401	0.0056
		205.76 (42−45)	6.0258	0.0077	254.68	4.8682	0.0000	195.43 (42−44)	6.3441	0.0019
		205.52 (40−43)	6.0328	0.0162	250.25	4.9544	0.0110	192.09 (39−43)	6.4546	0.0031
		201.39 (39−43)	6.1565	0.0003	249.83	4.9626	0.0000	191.60 (40−43)	6.4711	0.0278
					Water					
254.59	4.8700	255.11 (42−43)	4.8601	0.1921	266.56	4.6513	0.0000	233.01 (42−43)	5.3209	0.1588
291.00	4.2606	244.09 (41−43)	5.0795	0.0076	264.39	4.6894	0.2248	228.29 (41−43)	5.4311	0.0658
		238.74 (42−44)	5.1932	0.0032	257.26	4.8193	0.2215	219.59 (42−45)	5.6461	0.0052
		205.59 (42−45)	6.0306	0.0116	254.76	4.8666	0.0000	195.30 (42−44)	6.3484	0.0019
		205.35 (42−45)	6.0376	0.0128	249.94	4.9605	0.0100	191.93 (39−43)	6.4598	0.0043
		201.26 (39−43)	6.1604	0.0003	249.52	4.9689	0.0000	191.58 (40−43)	6.4715	0.0270
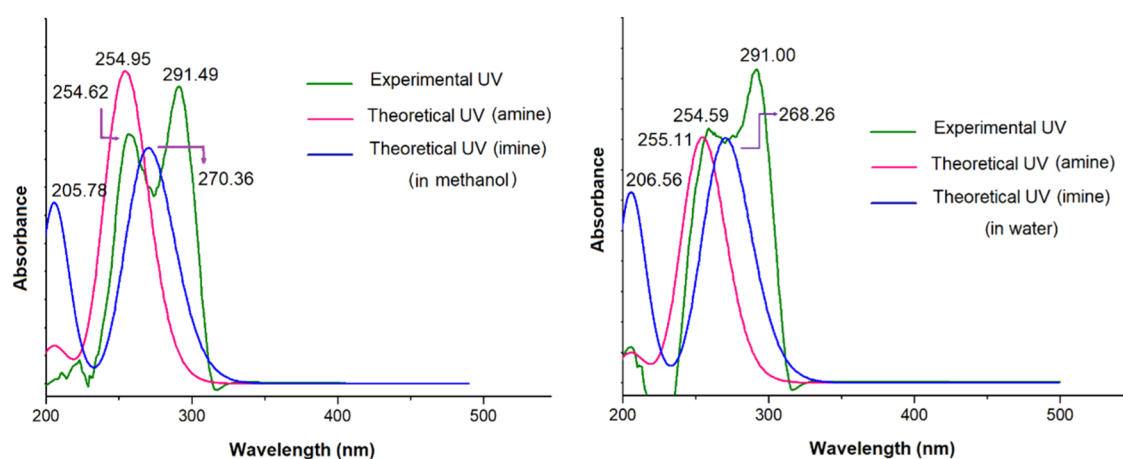
Figure 3. Experimental and theoretical UV spectrum of ATFT in methanol and water.

Table 4. Calculated Global Reactivity Descriptors of 1,3,4-Thiadiazole, DFTA, and ATFT at the B3LYP/6-311++G(d,p) Level

descriptor	1,3,4-thiadiazole	DFTA	ATFT
ionization potential I (eV)	9.76299	8.87885	9.02455
electron affinity A (eV)	−0.31344	0.21333	0.39850
electronegativity χ (eV)	4.72483	4.54610	4.71152
chemical potential μ_{cp} (eV)	−4.72489	−4.54620	−4.71160
chemical hardness η (eV)	5.03816	4.33276	4.31302
global softness S (eV^{-1})	0.19849	0.23080	0.23186
global electrophilicity index ω (eV)	2.21549	2.38498	2.57342

debye in methanol and 7.0857 debye in water (Table 2), implying the presence of strong intermolecular interactions in methanol and water solvents. The electric polarizability and hyperpolarizability are very significant parameters to anticipate the nonlinear optical conduct of the compounds. Moreover, polarizability has a direct correlation with the binding tendency of the ligand; a highly polarizable ligand is conceivable to bind more strongly to its target as compared to a weakly polarizable ligand.[68] The mean polarizability and the total first static hyperpolarizability (β_{total}) at M06-2X/B3LYP are estimated to be $(10.834/11.420) \times 10^{-24}$ e.s.u. and $(1.300/1.480) \times 10^{-30}$ e.s.u, respectively (Table 5). High polarizability value estimation of the title compound may enhance its bioactivity. It is noted that both polarizability and hyperpolarizability

values for the title compound are nearly the same at M06-2X and B3LYP.

3.5. NBO Analysis. To envisage the intra- and intermolecular bonding interactions, the NBO analysis[69] on the title compound at B3LYP/6-311++G(d,p) has been performed, and the details providing the charge transfer between electron donor and acceptor orbitals, the stabilization energy arising due to the conjugative interaction employing second-order perturbation theory, are presented in Table 6.

In the title molecule, the π electrons of (N2−C5) conjugated with π*(N1−C4) result in an energy of 16.17 kcal/mol for B3LYP and 21.64 kcal/mol for M06-2X. Interaction of LP1 (N6) with antibonding π*(N2−C5) results in the stabilization energy of 40.73/47.80 kcal/mol for B3LYP/M06-2X, which is also indicated by a decrease in occupancy from 2.000e to 1.79471e, thus representing a departure from the ideal Lewis structure. LP2 (S3) also shows notable interaction energies of 24.64 and 28.48 kcal/mol with antibonding π*(N1−C4) and π*(N2−C5), respectively, for B3LYP functional. The interaction electron lone pairs on fluorine atoms with adjacent antibonding σ(C−F) further stabilizes the system. Investigation of natural hybrid orbitals (NHOs) in terms of hybrid directionality and bond bending infers to the steric and substituent effects. From Table S1, it is evident that for N1 and C4, the NHOs of σ(N1−C4) are far from the line of center by ∼2°. In σ(C9−F10), the carbon (C9) shows a deviation of 1.2°. In σ(S3−C4) and σ(S3−C5),

Table 5. Polarizability and First Hyperpolarizability Data for ATFT Calculated at 6-311++G(d,p)

	polarizability			hyperpolarizability	
	B3LYP	M06-2X		B3LYP	M06-2X
α_{xx}	101.999	95.487	β_{xxx}	213.991	196.374
α_{xy}	0.225	0.535	β_{xxy}	25.033	−15.096
α_{yy}	78.723	75.226	β_{xyy}	−52.903	−42.707
α_{xz}	−0.273	−0.410	β_{yyy}	74.697	−53.139
α_{yz}	−0.052	−0.058	β_{xxz}	−15.239	7.0724
α_{zz}	50.444	48.598	β_{xyz}	−1.628	−1.942
α_{mean} (a.u.)	77.055	73.104	β_{yyz}	−7.462	4.976
α_{mean} (e.s.u.) × 10^{-24}	11.420	10.834	β_{xzz}	−43.816	−33.393
			β_{yzz}	21.768	−20.908
			β_{yzz}	−6.026	2.550
			β_{tot} (a.u.)	171.288	150.417
			β_{tot} (e.s.u.) × 10^{-30}	1.480	1.300

Table 6. Second-Order Perturbation Theory Analysis of Fock Matrix in NBO Basis for ATFT[b]

donor (i)	type	ED(i)(e) B3LYP (M06-2X)	acceptor (j)	type	ED(j)(e)[a] B3LYP (M06-2X)	E(2) kcal/mol B3LYP (M06-2X)	E(j) − E(i)[c] (a.u.) B3LYP (M06-2X)	F(i,j)[d] (a.u.) B3LYP (M06-2X)
N1−N2	σ	1.97770 (1.97770)	C5−N6	σ*	0.02422 (0.02481)	4.81 (5.45)	1.28 (1.43)	0.070 (0.079)
N1−C4	π	1.92292 (1.92782)	N2−C5	π*	0.39719 (0.37747)	8.35 (10.85)	0.33 (0.43)	0.051 (0.666)
N1−C4	π	1.92292 (1.92782)	C9−F12	σ*	0.10464 (0.09188)	5.50 (5.89)	0.56 (0.72)	0.050 (0.058)
N2−C5	π	1.86853 (1.87862)	N1−C4	π*	0.31550 (0.29838)	16.17 (21.64)	0.32 (0.43)	0.068 (0.090)
S3−C4	σ	1.97544 (1.97630)	C5−N6	σ*	0.02422 (0.02481)	5.72 (6.35)	1.12 (1.26)	0.071 (0.080)
N6−H7	σ	1.98061 (1.98066)	S3−C5	σ*	0.08291 (0.07419)	6.50 (7.44)	0.84 (0.97)	0.067 (0.077)
N1	LP(1)	1.89502 (1.90681)	C4	RY*(1)	0.00916 (0.00907)	4.88 (5.16)	1.25 (1.36)	0.071 (0.076)
N1	LP(1)	1.89502 (1.90681)	N2−C5	σ*	0.03123 (0.03016)	5.35 (6.08)	0.93 (1.08)	0.064 (0.073)
N1	LP(1)	1.89502 (1.90681)	S3−C4	σ*	0.07776 (0.06680)	15.81 (18.63)	0.55 (0.69)	0.084 (0.102)
N2	LP(1)	1.89800 (1.90878)	C5	RY*(1)	0.00922 (0.00920)	5.43 (5.95)	1.22 (1.30)	0.074 (0.080)
N2	LP(1)	1.89800 (1.90878)	N1−C4	σ*	0.02600 (0.02491)	5.27 (6.01)	0.96 (1.10)	0.065 (0.074)
N2	LP(1)	1.89800 (1.90878)	S3−C5	σ*	0.08291 (0.07419)	15.20 (18.23)	0.55 (0.68)	0.082 (0.100)
S3	LP(2)	1.65232 (1.65621)	N1−C4	π*	0.31550 (0.29838)	24.64 (34.11)	0.26 (0.34)	0.071 (0.097)
S3	LP(2)	1.65232 (1.65621)	N2−C5	π*	0.39719 (0.37747)	28.48 (38.44)	0.25 (0.32)	0.076 (0.101)
N6	LP(1)	1.79471 (1.81761)	N2−C5	π*	0.39719 (0.37747)	40.73 (47.80)	0.29 (0.39)	0.102 (0.128)
F10	LP(2)	1.95469 (1.95844)	C4−C9	σ*	0.06586 (0.06562)	5.49 (6.56)	0.77 (0.93)	0.058 (0.070)
F10	LP(2)	1.95469 (1.95844)	C9−F12	σ*	0.10464 (0.09188)	4.25 (5.13)	0.65 (0.85)	0.048 (0.060)
F10	LP(3)	1.93965 (1.94390)	C9−F11	σ*	0.08374 (0.07612)	10.11 (12.23)	0.68 (0.87)	0.074 (0.092)
F10	LP(3)	1.93965 (1.94390)	C9−F12	σ*	0.10464 (0.09188)	9.84 (11.43)	0.65 (0.84)	0.072 (0.088)
F11	LP(1)	1.99050 (1.99083)	C9	RY*(1)	0.01400 (0.01406)	7.33 (7.31)	2.21 (2.42)	0.114 (0.119)
F11	LP(2)	1.94606 (1.95071)	C4−C9	σ*	0.06586 (0.06562)	6.64 (7.93)	0.77 (0.93)	0.064 (0.077)
F11	LP(2)	1.94606 (1.95071)	C9−F12	σ*	0.10464 (0.09188)	6.25 (7.21)	0.65 (0.84)	0.058 (0.070)
F11	LP(3)	1.93355 (1.93842)	C9−F10	σ*	0.09911 (0.08792)	12.72 (14.98)	0.65 (0.84)	0.082 (0.101)
F11	LP(3)	1.93355 (1.93842)	C9−F12	σ*	0.10464 (0.09188)	9.52 (11.16)	0.65 (0.84)	0.071 (0.087)
F12	LP(2)	1.95205 (1.95584)	C4−C9	σ*	0.06586 (0.06562)	5.68 (6.86)	0.77 (0.93)	0.059 (0.072)
F12	LP(2)	1.95205 (1.95584)	C9−F11	σ*	0.08374 (0.07612)	4.79 (5.36)	0.67 (0.86)	0.051 (0.061)
F12	LP(3)	1.93905 (1.94307)	C9−F10	σ*	0.09911 (0.08792)	10.87 (12.75)	0.65 (0.84)	0.076 (0.093)
F12	LP(3)	1.93905 (1.94307)	C9−F11	σ*	0.08374 (0.07612)	9.23 (11.28)	0.67 (0.86)	0.071 (0.088)
			DIMER (B3LYP)					
N6	LP1	1.87544	H23−N17	σ*	0.05017	17.09	0.82	0.108
			DIMER (M06-2X)					
N6	LP1	1.88853	H23−N17	σ*	0.04326	17.49	0.97	0.118

[a]ED: electron density. [b]E(2): mean energy of hyperconjugative interactions. [c]Energy difference between the donor and acceptor i and j NBOs. [d]F(i,j) is the Fock matrix element between the i and j NBOs.

S3 NHOs show very large deviations of 10.4 and 9.6° with the line of nuclear centers, which result in a slightly stronger interaction between the lone pair of the corresponding nitrogen atoms and antibonding σ(C−S) orbitals.

3.6. Strength of Hydrogen Bonding. As the molecules of the title compound are linked into centrosymmetric dimers by paired N−H···N hydrogen bonds, we have estimated the strength of hydrogen bonding using NBO analysis of dimers as well as by topological studies in the topological analysis; the first and foremost step is to obtain the bond critical points (BCPs) between two adjacent atoms,[36] and after locating the BCPs, appropriate properties such as charge density (ρ_{BCP}), $\nabla^2\rho_{BCP}$, and ellipticity can be easily calculated at their position in space. The topological parameters for N−H···N hydrogen bonding for the title molecule are given in Table S2. The energy of N−H···N hydrogen bonds can be calculated using the relation as given by Espinosa et al.[70] In the case of the dimer, E_{HB} has been calculated to be 7.0720 kcal/mol at B3LYP and a slightly stronger bond is predicted by M06-2X with values at 7.6556 kcal/mol by topological analysis. Two negative (λ_1 and λ_2) and one positive (λ_3) eigenvalues for the BCP corresponding to the intermolecular hydrogen bonding also satisfy the criterion for hydrogen bonding.[36]

To estimate the strength of intermolecular hydrogen bonding, NBO analysis of the dimer of the title compound was also carried out. The charge transfer from nitrogen (N6) (LP1) lone pair to σ*(N17−H23) results in the occupancy of 0.05017e, and a strong hydrogen bonding (N17−H23···N6) interaction energy of 17.09/17.49 kcal mol^{−1} has been calculated at the B3LYP/M06-2X functional.

3.7. Vibrational Spectra Analysis. The optimized molecular geometry of ATFT shows the C_1 symmetry, which implies 30 active vibrational normal modes. The assignment of these vibrational modes has been performed at the B3LYP/6-311++G(d,p) level. The experimental FT-IR and FT−Raman wavenumbers along with the calculated theoretical wavenumbers (scaled) along with their PED are given in Table 7. All the 30 fundamental modes of vibrations are IR and Raman active, and therefore, the assignments for these vibrational modes have been done by considering their relative intensities, line shape, and PED obtained from the normal coordinate analysis. Overestimation of vibrational modes in DFT methods is expected because of the presence of anharmonicity in the real system, and hence, theoretically calculated harmonic wavenumbers are higher than the corresponding experimental wavenumbers. The disagreement between the theoretically

Table 7. Recorded (FT-IR and FT−Raman) Spectral Data and Computed Vibrational Wavenumbers along with the Assignments of Vibrational Modes Based on PED Results for ATFT[a]

s. no.	experimental wavenumbers		cal. waveno. (B3LYP)	cal. waveno. (M06-2X)	IR intensity B3LYP (M06-2X)	Raman activity B3LYP (M06-2X)	Raman intensity B3LYP (M06-2X)	[assignment of dominant modes at B3LYP*]
	FT-IR	FT−Raman						
1	3303 vs		3536	3529	55.59 (65.47)	51.28 (48.03)	10.4 (9.55)	νNH_2asym [97]
2	3129 vs		3425	3416	83.21 (93.52)	193.56 (173.79)	42.51 (37.52)	νNH_2sym [97]
3	1643 s	1644 w	1615	1566	181.65 (224.99)	12.74 (18.02)	12.08 (17.66)	NH_{2sciss} [53]+ νC5−N6 [21]
4	1515 vs	1512 s	1515	1526	21.65 (71.56)	31.15 (36.17)	32.63 (36.95)	νC=N(R) [93]
5		1495 s	1497	1478	258.85 (146.58)	53.50 (35.55)	57.16 (38.11)	νC=N(R) [85]
6	1316 s	1323 m	1315	1308	215.71 (342.99)	1.73 (1.35)	2.24 (1.75)	νC−F_3asym [75]
7	1305 sh		1286	1285	122.46 (27.93)	6.70 (3.62)	8.98 (4.79)	δ_{ip}R [55]+ νC4−C9 [15]
8	1190 vs	1182 m	1169	1200	130.73 (223.95)	13.47 (2.62)	20.71 (3.82)	νN−N(R) [51]+ β(C9−C4−N1) [23]
9	1150 vs	1141 s	1124	1144	168.23 (285.00)	34.84 (4.98)	56.64 (7.8)	νN−N(R) [40]+ NH_2 rock [25]
10		1076 vw	1088	1132	296.91 (82.98)	2.65 (31.55)	4.52 (50.1)	νC−F_3asym [80]
11	1040 vs	1038 m	1038	1030	50.11 (31.02)	2.91 (2.06)	5.29 (3.73)	NH_2 rock [56]+ νN−N [15]
12	1016 sh		1006	1010	205.09 (188.40)	3.04 (1.81)	5.77 (3.37)	δ_{ip}R [52]+ νC−F_3sym [41]
13	800 m	815 s	781	770	3.02 (1.13)	5.27 (4.69)	14.12 (12.65)	δ_{ip}R [68]+ νC5−N6 [11]
14	743 m	745 vs	718	722	23.31 (32.06)	13.59 (10.48)	40.86 (30.83)	δ_{sym}C−F_3 [70] (umbrella bending) + νC−S(R) [22]
15	683 m	682 vs	641	652	8.59 (6.72)	7.64 (8.48)	26.71 (28.61)	νC−S(R) [55]+ β(N6−C5−N2) [23]
16	614 m	621 m	627	623	2.83 (5.06)	1.66 (1.12)	5.99 (4.02)	τR [85]
17	573 sh		620	613	14.04 (22.79)	0.96 (1.28)	3.52 (4.71)	τR [91]
18			611	602	5.90 (11.30)	1.80 (1.56)	6.72 (5.89)	τR [90]
19		558 m	535	536	10.89 (15.20)	2.14 (1.81)	9.61 (8.01)	δ_{asym}C−F_3 [51]+ NH_2 wag [16]
20	517 m		531	527	13.83 (37.23)	0.98 (1.12)	4.42 (5.04)	τR [37]+ νC−S(R) [26] + δ_{asym}C−F_3 [15]
21	431 m		469	479	174.91 (169.85)	1.25 (1.94)	6.74 (10.05)	NH_2 wag [57]+ τ_1R [21]
22			411	408	60.45 (47.53)	1.25 (1.28)	8.16 (8.32)	δ_{asym}C−F_3 [25]+ NH_2 wag [15] + τR [10]
23		429 vs	402	395	1.04 (1.26)	5.81 (4.45)	39.08 (30.32)	β(N6−C5−S3) [55]+ δ_{asym}C−F_3 [15]
24		362 m	335	329	0.74 (0.21)	0.41 (0.41)	3.65 (3.62)	β(N2−C5−N6) [61]+ δ_{asym}C−F_3 [11]
25		325 vs	311	307	1.07 (1.26)	4.84 (4.54)	47.95 (44.95)	τR−NH_2 [45]+ C−F_{3rock1} [33]
26			300	282	54.04 (46.24)	0.41 (0.56)	4.32 (6.32)	NH_2 twisting [63]
27		240 m	229	225	4.26 (5.03)	0.24 (0.22)	3.82 (3.52)	τC5−NH_2 [43]+ τR [22] + C−F_{3rock1} [28]
28			151	146	2.66 (2.54)	0.41 (0.34)	12.96 (11.3)	β(C9−C4−S3) [40]+ C−F_{3rock1} [11]
29			96	96	1.20 (0.94)	2.71 (2.44)	190.36 (172.89)	τR-CF_3 [50]+ τR-NH_2 [48]
30			14	21	2.52 (2.60)	1.83 (1.63)	5231.94 (2138.28)	τC4−C9 [50]+ NH_2 twisting [20]

[a]R, thiadiazole ring; ν, stretching; sym, symmetric; asym, asymmetric; sciss, scissoring; ip, in plane; δ, deformation; β, in-plane bending; wag, wagging; rock, rocking; and τ, torsion; PED below 10% not taken into consideration.

calculated and experimental wavenumbers has been rectified by the use of a proper scaling factor, and the scaled wavenumbers show good conformity with the experimental spectra. The wavenumbers quoted in the discussion corresponds to the B3LYP functional, where M06-2X wavenumbers are specifically mentioned. The experimental FT-IR and FT−Raman spectra and the corresponding simulated vibrational spectra of the monomer are plotted together in Figure 4.

The title compound consists of a thiadiazole ring having an amino group attached at position 5 and a trifluoromethyl group at position 4, and hence, a detailed vibrational analysis is conferred under three heads: (i) amino group vibrations, (ii) thiadiazole ring vibrations, and (iii) trifluoromethyl group vibrations.

3.7.1. Amino Group Vibrations. Primary amines have two N−H stretching bands in the regions around 3520−3420 and 3420−3340 cm^{-1}, a broad strong NH_2 scissoring band around 1590−1630 cm^{-1}, NH_2 rocking around 1150−1000 cm^{-1}, and NH_2 wagging and twisting bands in the 850−750 cm^{-1} range.[71] Because of the presence of intermolecular hydrogen

bonding, the NH_2 asymmetric and symmetric stretching vibrations were expected at a lower range with obvious deviation in experimental and theoretical wavenumbers. The absorption in this particular region is highly dependent on the degree of hydrogen bonding.[72] For the title compound, the NH_2 asymmetric stretching and symmetric stretching are calculated at 3536 and 3425 cm^{-1}. The corresponding experimental FT-IR wavenumbers are observed at 3303 and 3129 cm^{-1}. This noticeable deviation for NH stretching vibrations has also been reported for intermolecular hydrogen-bonded systems.[73]

A distinct NH_2 scissoring mode is observed at 1643 and 1644 cm^{-1} in the FT-IR and FT−Raman spectra, respectively, while a sharp peak at 1615 cm^{-1} in the theoretical IR spectrum is assigned to this mode. The wavenumber corresponding to NH_2 scissoring at the M06-2X functional shows a slight deviation from the corresponding experimental mode. A strong peak at 1040 cm^{-1} in FT-IR spectra and a medium peak at 1038 cm^{-1} in FT−Raman spectra have been assigned to the NH_2 rocking mode with the corresponding theoretically
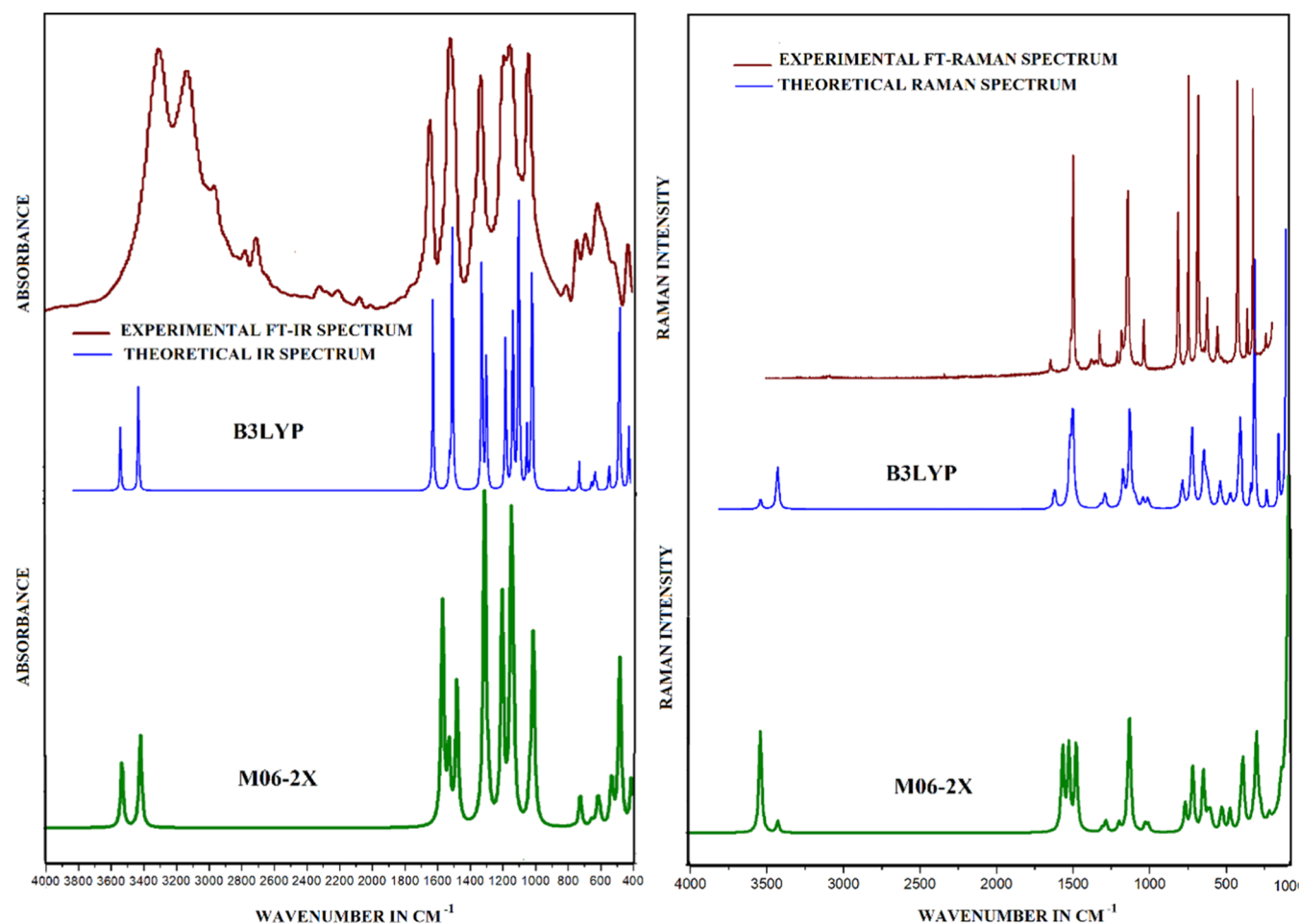
Figure 4. Experimental and theoretical IR and Raman spectra of ATFT at B3LYP and M06-2X.

calculated peak at 1038 cm^{-1} (56% P.E.D.) and mixed with N−N stretching vibration (15% PED). Another mode at 1124 cm^{-1} is a similar mixed mode with a dominance of N−N stretching. The rocking motion of the NH$_2$ group in 2-acetamido-5-aminopyridine has been observed at 1120/1115 cm^{-1} in the FT-IR/Raman spectrum as a medium/weak band.[74]

Although the NH$_2$ wagging vibration is so invincibly anharmonic quite similar to the inversion mode of NH$_3$, that it is not possible to reproduce it correctly by the harmonic treatment,[75] our calculations predict this wagging vibration at 469/479 cm^{-1} at B3LYP/M06-2X. The NH$_2$ twisting mode is calculated at 300 cm^{-1} with 63% PED. The NH$_2$ twisting mode has been assigned at 315 cm^{-1} in the case of 5-aminouracil[76] and as a weak shoulder band in the Raman spectrum at 235 cm^{-1} for 2-acetamido-5-aminopyridine.[74]

3.7.2. Thiadiazole Ring Vibrations. The vibrations of a five-membered hetero thiadiazole ring involve C−S, C═N, and N−N stretching vibrations and the corresponding angle bending modes and torsions of the ring. Because of the presence of three heteroatoms and the conjugated bond −C═N−N═C−S− system in the ring, vibrations involving heteroatoms are modified and altered. The C−S stretching vibration, which is of variable intensity and observed over the wide region 1035−245 cm^{-1},[77] does not give a sharp and strong band in infrared, and as such, assignment is not easy in the infrared but gives a discernible band in the Raman spectrum.[78] The experimental C−S stretching spectral peaks

for the title compound are observed at 683 (IR) m/682 (R) vs (m = medium, vs = very strong), 517 cm^{-1} (IR) m, and the corresponding theoretical modes of the thiadiazole ring with two C−S bonds are calculated at 641 and 531 cm^{-1}. These vibrations have a significant contribution from C−S stretching along with other vibrations of the ring and/or the trifluoromethyl group. Two C−N stretching vibrations are observed at 1515/1512 and 1495 cm^{-1} as strong bands in the FT-IR/FT−Raman spectra and the corresponding theoretically assigned values are at 1515 and 1497 cm^{-1}. In the IR spectrum of 2-amino-5-phenyl-1,3,4-thiadiazole, two peaks at 1489 and 1465 cm^{-1} have been assigned as the C−N stretching modes.[79] The C−N stretching mode is also in line with the modes calculated at 1494 and 1475 cm^{-1} for 5-(4-pyridinyl)-1,3,4-thiadiazol-2-amine by Shukla *et al.*[80]

The N−N stretching vibration of the thiadiazole ring is observed as a medium to a strong band in the Raman and IR spectrum in the range 1200−1100 cm^{-1}. For 5-(4-pyridinyl)-1,3,4-thiadiazol-2-amine,[80] a very strong band in the FT−Raman spectrum at 1133 cm^{-1} and a medium intense band at 1141 cm^{-1} in the FT-IR spectrum are assigned to the N−N stretching of the thiadiazol ring. Bezerra *et al.*[81] have assigned it at 1121 cm^{-1} and Crane *et al.*[82] at 1151 cm^{-1}. In the Raman spectrum of N-phenyl-5-phenyl-1,3,4-thiadiazole-2-amine,[83] N−N stretching vibrations are observed at 1149 and 1103 cm^{-1}, and the corresponding IR peaks are reported at 1141 and 1100 cm^{-1}. For the title compound, we have observed two very strong bands at 1190 (1182) and 1150 (1141) cm^{-1} in
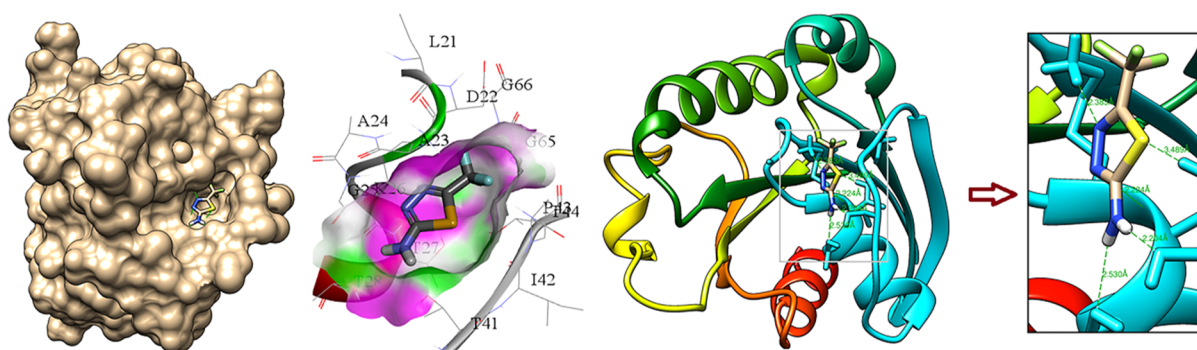
Figure 5. Docking of ATFT in the binding site of 2W83 and formation of hydrogen bonding.

the FT-IR (FT−Raman) spectra as N−N stretching vibrations of the thiadiazole ring. In-plane ring deformation and torsional mode of the thiadiazole ring are also well matched with the experimental peaks.

3.7.3. Trifluoromethyl Group Vibrations. The title compound contains a CF_3 group attached with one carbon atom of the thiadiazole ring. The fundamental vibrations associated with the CF_3 group are symmetric and asymmetric stretching, bending, rocking, and torsional modes. The three fluorine atoms greatly shift the stretching wavenumbers below 1300 cm^{-1}.[84] For benzene derivatives holding the C−CF_3 group, the C−F stretching vibrations are identified in the range 1360−1300 cm^{-1}.[85] The mode is expected to be at lower wavenumbers for thiadiazole derivatives with the CF_3 moiety. The calculated asymmetric and symmetric C−F stretching modes in the present case are at 1315, 1088, and 1006 cm^{-1}. These modes are in coherence with the observed experimental peaks. The CF_3 symmetric or umbrella bending is observed at 743/745 in IR/Raman and calculated at 718 cm^{-1}. A medium intensity band at 558 cm^{-1} in Raman spectra is assigned to the CF_3 asymmetric deformation vibrations in good agreement with the theoretical peak at 535 cm^{-1} with 51% contribution to PED. The CF_3 in-plane and out-of-plane rocking vibrations assigned at 311 and 229 cm^{-1} and observed at 325 and 240 cm^{-1} in the Raman spectrum are in line with the literature.[86]

3.8. Thermodynamic Properties. Computation of thermodynamic properties and their variation with temperature are fairly important in the field of thermochemistry and chemical equilibrium.[87−89] For the computation of thermodynamic parameters, Gaussian software adopts the noninteracting particle model and the ideal gas approximation. The equations used for the computation of thermodynamic properties are in line with the standard texts on thermodynamics.[87] Important thermodynamic functions such as entropy, enthalpy changes, and heat capacity at various temperatures (100−400 K) are obtained from the theoretical vibration analysis (Table S3). The corresponding fitting equations for the title molecule are as follows and the correlation graphics are shown in Figure S3.

$$C_{p,m}^0 \text{ (cal/mol-kelvin)}$$
$$= -7.0000 \times 10^{-5}T^2 + 0.1205T + 4.5901 \ (R^2$$
$$= 0.9996)$$

$$S_{p,m}^0 \text{ (cal/mol-kelvin)}$$
$$= -6.0000 \times 10^{-5}T^2 + 0.1523T + 56.216 \ (R^2$$
$$= 0.9999)$$

$$\Delta H_{p,m}^0 \text{ (kcal/mol)}$$
$$= 3.0000 \times 10^{-5}T^2 + 0.0152T - 0.7917 \ (R^2$$
$$= 0.9997)$$

As the thermodynamic computations pertain to the gas phase, these cannot be used in the solution.

3.9. ADME Parameters. Computation of the pharmacological properties of absorption, distribution, metabolism, and excretion (ADME) of a molecule is crucial for its initial selection as a drug candidate and set standards for the evaluation of compounds synthesized during lead optimization. During lead optimization, further improvements in ADME properties are attempted while preserving the molecule's potency and selectivity. The computational prediction of pharmacokinetics, drug-likeness, and bioavailability was carried out using the online tool SwissADME.[90] To detect drug-likeness, the tool predicts bioavailability radar (the pink-colored zone represents a suitable physicochemical space for oral bioavailability) as per six physicochemical properties such as size, polarity, solubility, flexibility, saturation, and lipophilicity. The topological polar surface area and the lipophilicity parameters iLOGP, XLOGP, WLOGP, and MLOGP of ATFT are calculated to be 80.04 Å^2, 1.05, 0.94, 2.3, and 0.21, respectively. The bioavailability score is calculated to be 0.55 with high gastrointestinal (GI) absorption. The compound lies well within the pink space (Figure S4) and satisfies the Lipinski rule of five,[91] the Veber rule,[92] as well as the Egan rule[93] suggesting that ATFT theoretically has good bioavailability.

3.10. Molecular Docking. The optimized structure of the title compound at B3LYP/6-311++G (d,p) was used as the ligand. The protein and ligand files were prepared in a pdbqt format. The Auto Grid "grid box" was utilized for the network of grid map. The grid size was set to 33 × 28 × 31 *xyz* points with a grid spacing of 0.375 Å, and the grid center was selected at (*x*, *y*, and *z*) 48.05, −13.14, and 16.74, respectively. During the docking procedure, both the proteins and ligands were considered as rigid. According to the molecular docking simulation results on 2W83, out of 10 poses, one pose with a binding affinity of −5.5 kcal/mol was obtained forming five hydrogen bonds with the neighboring residues. The protein−ligand binding pocket docked ligand and hydrogen bonding with the nearby residues are shown in Figure 5. The donor and acceptor atoms and the hydrogen bonding distance are given in Table S4. The docking results and the formation of a good number of hydrogen bonds suggested that the title compound appears to be a promising anticancer agent. The ADME
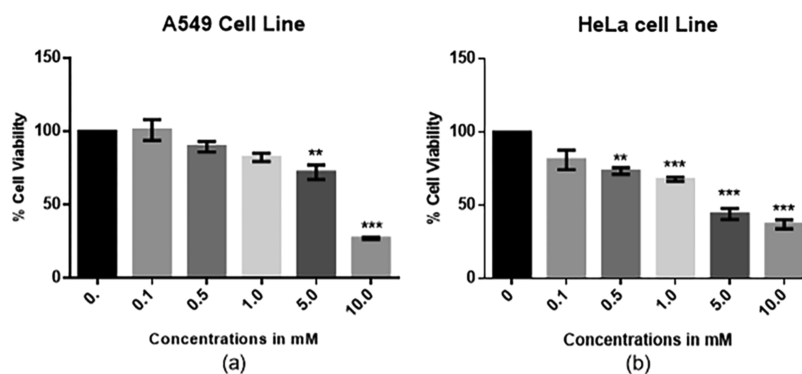
Figure 6. Effect of the extracts on cell viability and proliferation.

parameters and molecular docking prompted us to analyze the biological activity against cancer cell lines.

3.11. Evaluation of Cytotoxic Activity. Cytotoxicity of ATFT was measured as percent cell viability at different concentrations of the compound. The viability of cancer cells was reduced to a significant level with concentrations of ATFT when compared to untreated cells (Figure 6). ATFT showed the highest cytotoxicity at 5 mM and 10 mM and least at 0.5 mM concentration in both cell lines. The IC_{50} represents the concentration of a drug that is required for 50% inhibition *in vitro*, that is, IC_{50} for A549 cells is 5.7 mM and for HeLa cells is 5.1 mM. However, no effect was observed in untreated cells and solvent control.

4. CONCLUSIONS

In the present investigation, the spectroscopic profile of the title compound has been analyzed using DFT (B3LYP and M06-2X) in conjunction with the experimental FT−Raman and FT-IR techniques. A convincing concordance between the experimental and calculated normal modes of vibrations has been observed. The rotational barrier of the NH_2 group as well as the conversion of amine to imine tautomer along with the transition state for the title compound has been calculated to be 6.08056 kcal/mol and 44.47788 kcal/mol respectively. The much higher barrier corresponding to the conversion between amine and imine tautomer ruled out the possibility of imine tautomer in solid state. The high polarizability value at both M06-2X and B3LYP may enhance its bioactivity. The energy of N−H···N hydrogen bonds using topological analysis has been calculated to be 7.0720/7.6556 kcal/mol at B3LYP/M06-2X. Molecular docking simulation results on cancer-active protein 2W83 show the formation of five hydrogen bonds with the neighboring residues with binding affinity −5.5 kcal/mol. Analysis of the anticancer activity of the title compound based on the ability to inhibit the proliferation of A549 and HeLa cancer cell lines shows positive results as the viability of cancer cells was reduced to a significant level with concentrations of ATFT when compared to untreated cells.

5. EXPERIMENTAL SECTION

5.1. Sample and Spectroscopic Measurements. The title compound (in powder form) was procured from Sigma-Aldrich Chemical Company (USA) with a purity of 97% and was used intrinsically for spectroscopic analysis. For optical characterization of the molecule, a UV Evolution 302 spectrometer and a Shimadzu 8700 1992 infrared spectrometer were used. The FT-IR spectrum (spectral resolution of 0.5

cm^{-1}) was recorded on a Varian 7000 series spectrometer in the region 4000−400 cm^{-1}. The Raman spectrum was recorded on a Raman spectrometer (Renishaw) using 785 nm Ar^+ with 0.1% of the total power of the laser in the range 3500−200 cm^{-1}.

5.2. Cell Lines for Biological Activity. Two adherent cancer cell lines, human lung cancer (A549) and cervical cancer (HeLa) supplied by the National Center for Cell Sciences (NCCS) Cell Repository, Pune, India, were used in the experiment.

5.3. Biological Activity. The cytotoxic effect of ATFT was checked on both human lung cancer cell line (A549) and human cervical cancer cell line (HeLa).

5.3.1. Cell Culture. Both cell lines were maintained and propagated in Dulbecco's modified Eagle's medium supplemented with 2 mM L-glutamine and 10% v/v fetal bovine serum. Cells were placed in a CO_2 incubator at 37 °C and a humidified atmosphere of 5% (v/v) CO_2, until the cells become 80% confluent. The cultured cells were rinsed in 0.01 M phosphate-buffered saline, trypsinized with trypsin−ethylenediaminetetraacetic acid solution, and resuspended in the culture medium. The cells were seeded at a density of 2×10^6 cells/ml of solution. After 24 h in culture, the cells were used in subsequent exposure experiments.

5.3.2. Cell Viability. The cell viability of untreated and treated cells was assessed by the tetrazolium dye 3-(4,5-dimethylthiazol-2-yl)-2,5-diphenyltetrazolium bromide (MTT) (Himedia, Pennsylvania, USA) reduction assay as described by Mosmann.[94] Briefly, cells were plated in a 96-well plate (1×10^4 cells/well), treated with different concentrations (0−10 mM) of the compound, and incubated at 37 °C in a 5% CO_2 incubator for 24 h. After incubation, MTT (0.5 mg/mL) was added to each well and incubated at 37 °C for 4 h. Thereafter, the media were removed and 100 μL of dimethyl sulfoxide was added to dissolve the formazan crystals. The plate was read at 540 nm using a microplate reader (BIO-RAD model 680), and cell viability was calculated as percent cell viability. Statistical analysis was done using GraphPad Prism (ver. 6.0).

The anticancer activity of the concerned molecule was evaluated *in vitro* based on their ability to inhibit the proliferation of A549 and HeLa cell lines; for this, a standard MTT microplate assay with MTT (Sigma Aldrich) was used.

■ ASSOCIATED CONTENT

ⓈI Supporting Information

The Supporting Information is available free of charge at https://pubs.acs.org/doi/10.1021/acsomega.0c04474.

Rotation barrier corresponding to the NH_2 group and barrier corresponding to the conversion between imino and amino tautomer; MESP surface for ATFT calculated by the B3LYP/6-311++G(d,p) method; correlation graph of the calculated heat capacity, entropy, and change in enthalpy for the title molecule; bioavailability radar; NHO directionality and "bond bending" (deviations from the line of nuclear centers); topological parameters for hydrogen-bonded interactions in ATFT dimer; thermodynamic properties of ATFT calculated at different temperatures using the DFT-B3LYP/6−311++G(d,p) method; and hydrogen bond distance with a respective donor and acceptor atom (PDF)

AUTHOR INFORMATION

Corresponding Authors

Lamya H. Al-Wahaibi − *Department of Chemistry, College of Sciences, Princess Nourah bint Abdulrahman University, Riyadh 11671, Saudi Arabia*; Email: lhalwahaibi@pnu.edu.sa

Leena Sinha − *Department of Physics, University of Lucknow, Lucknow 226007, India*; orcid.org/0000-0003-3624-4085; Email: sinhaleena27@gmail.com

Authors

Isha Singh − *Department of Physics, University of Lucknow, Lucknow 226007, India*

Ruchi Srivastava − *Department of Physics, University of Lucknow, Lucknow 226007, India*

Onkar Prasad − *Department of Physics, University of Lucknow, Lucknow 226007, India*

Shilendra K. Pathak − *Department of Physics, M. M. M. P. G. College, Deoria 274702, India*

Saurabh Kumar − *Molecular & Human Genetics Lab, Department of Zoology, University of Lucknow, Lucknow 226007, India*

Shama Parveen − *Molecular & Human Genetics Lab, Department of Zoology, University of Lucknow, Lucknow 226007, India*

Monisha Banerjee − *Molecular & Human Genetics Lab, Department of Zoology, University of Lucknow, Lucknow 226007, India*

Ali A. El-Emam − *Department of Medicinal Chemistry, Faculty of Pharmacy, University of Mansoura, Mansoura 35516, Egypt*

Complete contact information is available at:
https://pubs.acs.org/10.1021/acsomega.0c04474

Notes

The authors declare no competing financial interest.

REFERENCES

(1) Bravo, P.; Diliddo, D.; Resnati, G. An efficient entry to perfluoroalkyl substituted azoles starting from *β*-perfluoroalkyl-*β*-dicarbonyl compounds. *Tetrahedron* **1994**, *50*, 8827−8836.

(2) Mei, H.; Han, J.; Fustero, S.; Medio-Simon, M.; Sedgwick, D. M.; Santi, C.; Ruzziconi, R.; Soloshonok, V. A. Fluorine-Containing Drugs Approved by the FDA in 2018. *Chem.—Eur. J.* **2019**, *25*, 11797−11819.

(3) Muller, K.; Faeh, C.; Diederich, F. Fluorine in Pharmaceuticals: Looking Beyond Intuition. *Science* **2007**, *317*, 1881−1886.

(4) Kees, L. L.; Fitzgerald, J. J.; Steiner, K. E.; Mattes, J. F.; Mihan, B.; Tosi, T.; Mondoro, D.; McCaleb, M. L. New Potent Antihyperglycemic Agents in db/db Mice: Synthesis and Structure−Activity Relationship Studies of (4-Substituted benzyl)(trifluoromethyl)pyrazoles and −pyrazolones. *J. Med. Chem.* **1996**, *39*, 3920−3928.

(5) Haranahalli, K.; Honda, T.; Ojima, I. Recent progress in the strategic incorporation of fluorine into medicinally active compounds. *J. Fluorine Chem.* **2019**, *217*, 29−40.

(6) Er, M.; Isildak, G.; Tahtaci, H.; Karakurt, T. Novel 2-amino-1,3,4-thiadiazoles and their acyl derivatives: Synthesis, structural characterization, molecular docking studies and comparison of experimental and computational results. *J. Mol. Struct.* **2016**, *1110*, 102−113.

(7) Gillis, E. P.; Eastman, K. J.; Hill, M. D.; Donnelly, D. J.; Meanwell, N. A. Applications of Fluorine in Medicinal Chemistry. *J. Med. Chem.* **2015**, *58*, 8315−8359.

(8) Romano, E.; Ladetto, M. F.; Brandán, S. A. Structural and vibrational studies of the potential anticancer agent, 5-difluoromethyl-1,3,4-thiadiazole-2-amino by DFT calculations. *Comput. Theor. Chem.* **2013**, *1011*, 57−64.

(9) Gujral, M. S.; Patnaik, P. M.; Kaul, R.; Parikh, H. K.; Conradt, C.; Tamhankar, C. P.; Daftary, G. V. Efficacy of hydrolytic enzymes in preventing radiation therapy-induced side effects in patients with head and neck cancers. *Cancer Chemother. Pharmacol.* **2001**, *47*, S23−S28.

(10) Stockler, M. R.; Wilcken, N. J. C.; Coates, A. S. Chemotherapy for advanced breast cancer − how long should it continue? *Breast Cancer Res. Treat.* **2003**, *81*, S49−S52.

(11) Foroumadi, A.; Soltani, F.; Moallemzadeh-Haghighi, H.; Shafiee, A. Synthesis,in vitro-Antimycobacterial Activity and Cytotoxicity of Some Alkyl ?-(5-aryl-1, 3, 4-thiadiazole-2-ylthio)acetates. *Arch. Pharm.* **2005**, *338*, 112−116.

(12) Mastrolorenzo, A.; Scozzafava, A.; Supuran, C. T. 4-Toluenesulfonylureido derivatives of amines, amino acids and dipeptides: a novel class of potential antitumor agents. *Eur. J. Pharm. Sci.* **2000**, *11*, 325−332.

(13) Senff-Ribeiro, A.; Echevarria, A.; Silva, E. F.; Veiga, S. S.; Oliveira, M. B. M. Antimelanoma activity of 1,3,4-thiadiazolium mesoionics: a structure-activity relationship study. *Anticancer Drugs* **2004**, *15*, 269−275.

(14) Rzeski, W.; Matysiak, J.; Kandefer-Szerszeń, M. Anticancer, neuroprotective activities and computational studies of 2-amino-1,3,4-thiadiazole based compound. *Bioorg. Med. Chem.* **2007**, *15*, 3201−3207.

(15) Remko, M.; Swart, M.; Bickelhaupt, F. M. Theoretical study of structure, pKa, lipophilicity, solubility, absorption, and polar surface area of some centrally acting antihypertensives. *Bioorg. Med. Chem.* **2006**, *14*, 1715−1728.

(16) Nelson, J. A.; Rose, L. M.; Bennett, L. L. Effects of 2-amino-1,3,4-thiadiazole on Ribonucleotide pools of leukemia L1210 cells. *Cancer Res.* **1976**, *36*, 1375−1378.

(17) Hill, D. L. Aminothiadiazoles. *Cancer Chemother. Pharmacol.* **1980**, *4*, 215−220.

(18) Matysiak, J.; Nasulewicz, A.; Pełczyńska, M.; Świtalska, M.; Jaroszewicz, I.; Opolski, A. Synthesis and antiproliferative activity of

some 5-substituted 2-(2,4-dihydroxyphenyl)-1,3,4-thiadiazoles. *Eur. J. Med. Chem.* **2006**, *41*, 475−482.

(19) Chou, J.-Y.; Lai, S.-Y.; Pan, S.-L.; Jow, G.-M.; Chern, J.-W.; Guh, J.-H. Investigation of anticancer mechanism of thiadiazole-based compound in human non-small cell lung cancer A549 cells. *Biochem. Pharmacol.* **2003**, *66*, 115−124.

(20) Radi, M.; Crespan, E.; Botta, G.; Falchi, F.; Maga, G.; Manetti, F.; Corradi, V.; Mancini, M.; Santucci, M. A.; Schenone, S.; Botta, M. Discovery and SAR of 1,3,4-thiadiazole derivatives as potent Abl tyrosine kinase inhibitors and cytodifferentiating agents. *Bioorg. Med. Chem. Lett.* **2008**, *18*, 1207−1211.

(21) Dogan, H. N.; Duran, A.; Rollas, S.; Sener, G.; Uysal, M. K.; Gülen, D. Synthesis of New 2,5-Disubstituted-1,3,4-thiadiazoles and Preliminary Evaluation of Anticonvulsant and Antimicrobial Activities. *Bioorg. Med. Chem.* **2002**, *10*, 2893−2898.

(22) Rollas, S.; Karakus, S.; Durgun, B. B.; Kiraz, M.; Erdeniz, H. Synthesis and antimicrobial activity of some 1,4-disubstituted thiosemicarbazide and 2,5-disubstituted 1,3,4-thiadiazole derivatives. *Farmaco* **1989**, *51*, 811−814.

(23) Demirbas, A.; Sahin, D.; Demirbas, N.; Karaoglu, S. A. Synthesis of some new 1,3,4-thiadiazol-2-ylmethyl-1,2,4-triazole derivatives and investigation of their antimicrobial activities. *Eur. J. Med. Chem.* **2009**, *44*, 2896−2903.

(24) Kadi, A. A.; El-Brollosy, N. R.; Al-Deeb, O. A.; Habib, E. E.; Ibrahim, T. M.; El-Emam, A. A. Synthesis, antimicrobial, and anti-inflammatory activities of novel 2-(1-adamantyl)-5-substituted-1,3,4-oxadiazoles and 2-(1-adamantylamino)-5-substituted-1,3,4-thiadia-zoles. *Eur. J. Med. Chem.* **2007**, *42*, 235−242.

(25) Shukla, H. K.; Desai, N. C.; Astik, R. R.; Thaker, K. A. Studies on some Thiosemicarbazones and 1, 3, 4-thiadiazolines as potential Antitubercular and Antibacterial Agents. *J. Indian Chem. Soc.* **1984**, *6*, 168−169.

(26) Mullican, M. D.; Wilson, M. W.; Conner, D. T.; Kostlan, C. R.; Schrier, D. J.; Dyer, R. D. Design of 5-(3,5-di-tert-butyl-4-hydroxyphenyl)-1,3,4-thiadiazoles, -1,3,4-oxadiazoles, and -1,2,4-tri-azoles as orally active, nonulcerogenic antiinflammatory agents. *J. Med. Chem.* **1993**, *36*, 1090−1099.

(27) Mathew, V.; Keshavayya, J.; Vaidya, V. P.; Giles, D. Studies on synthesis and pharmacological activities of 3,6-disubstituted-1,2,4-triazolo[3,4-b]-1,3,4-thiadiazoles and their dihydro analogues. *Eur. J. Med. Chem.* **2007**, *42*, 823−840.

(28) Turner, S.; Myers, M.; Gadie, B.; Nelson, A. J.; Pape, R.; Saville, J. F.; Doxey, J. C.; Berridge, T. L. Antihypertensive Thiadiazoles. 1. Synthesis of Some 2-Aryl-5-hydrazino-1,3,4-thiadiazoles with Vaso-dilator Activity. *J. Med. Chem.* **1988**, *31*, 902−906.

(29) Turner, S.; Myers, M.; Gadie, B.; Hale, S. A.; Horsley, A.; Nelson, A. J.; Pape, R.; Saville, J. F.; Doxey, J. C.; Berridge, T. L. Antihypertensive thiadiazoles. 2. Vasodilator activity of some 2-aryl-5-guanidino-1,3,4-thiadiazoles. *J. Med. Chem.* **1988**, *31*, 906−913.

(30) Chapleo, C. B.; Myers, P. L.; Smith, A. C. B.; Stillings, M. R.; Tulloch, I. F.; Walter, D. S. Substituted 1,3,4-thiadiazoles with anticonvulsant activity. 4. Amidines. *J. Med. Chem.* **1988**, *31*, 7−11.

(31) Rajak, H.; Behera, C. K.; Pawar, R. S.; Singour, P. K.; Kharya, M. D. A novel series of 2,5-disubstituted 1,3,4-thiadiazoles as potential anticonvulsant agent. *Chin. Chem. Lett.* **2010**, *21*, 1149−1152.

(32) Cressier, D.; Prouillac, C.; Hernandez, P.; Amourette, C.; Diserbo, M.; Lion, C.; Rima, G. Synthesis, antioxidant properties and radioprotective effects of new benzothiazoles and thiadiazoles. *Bioorg. Med. Chem.* **2009**, *17*, 5275−5284.

(33) Nkurunziza, J. B.; Kalluraya, B. Synthesis and Characterization of Novel Series of 1,2,4-Triazolo[3,4-b]-1,3,4-Thiadiazole Derivatives of Anilinoacetic Acids as Promising Antioxidant Agents. *Arc. Org. Inorg. Chem. Sci.* **2018**, *2*, 180−185.

(34) Mazzone, G.; Pignatello, R.; Mazzone, S.; Panico, A.; Pennisi, G.; Castana, R.; Mazzone, P. Synthesis and local anesthetic activity of alkylaminoacyl derivatives of 2-amino-1,3,4-thiadiazole. *Farmaco* **1993**, *48*, 1207−1224.

(35) Nomoto, Y.; Takai, H.; Hirata, T.; Teranishi, M.; Ohno, T.; Kubo, K. Studies on cardiotonic agents. V. Synthesis of 1-(6,7-dimethoxy-4-quinazolinyl)piperidine derivatives carrying various 5-membered heterocyclic rings at the 4-position. *Chem. Pharm. Bull.* **1991**, *39*, 86−90.

(36) Bader, R. F. W. A quantum theory of molecular structure and its applications. *Chem. Rev.* **1991**, *91*, 893−928.

(37) Kohn, W.; Sham, L. J. Self-Consistent Equations Including Exchange and Correlation Effects. *Phys. Rev.* **1965**, *140*, A1133−A1138.

(38) Becke, A. D. Density-functional thermochemistry. III. The role of exact exchange. *J. Chem. Phys.* **1993**, *98*, 5648−5652.

(39) Lee, C.; Yang, W.; Parr, R. G. Development of the Colle-Salvetti correlation-energy formula into a functional of the electron density. *Phys. Rev. B: Condens. Matter Mater. Phys.* **1998**, *37*, 785−789.

(40) Zhao, Y.; Schultz, N. E.; Truhlar, D. G. Exchange-correlation functional with broad accuracy for metallic and nonmetallic compounds, kinetics, and noncovalent interactions. *J. Chem. Phys.* **2005**, *123*, 161103.

(41) Sousa, S. F.; Fernandes, P. A.; Ramos, M. J. General Performance of Density Functionals. *J. Phys. Chem. A* **2007**, *111*, 10439−10452.

(42) Minenkov, Y.; Wang, H.; Wang, Z.; Sarathy, S. M.; Cavallo, L. Heats of Formation of Medium-Sized Organic Compounds from Contemporary Electronic Structure Methods. *J. Chem. Theory Comput.* **2017**, *13*, 3537−3560.

(43) Zhang, I. Y.; Wu, J.; Xu, X. Extending the reliability and applicability of B3LYP. *Chem. Commun.* **2010**, *46*, 3057−3070.

(44) Zhao, Y.; Truhlar, D. G. Design of Density Functionals That Are Broadly Accurate for Thermochemistry, Thermochemical Kinetics, and Nonbonded Interactions. *J. Phys. Chem. A* **2005**, *109*, 5656−5667.

(45) Schreiner, P. R.; Fokin, A. A.; Pascal, R. A.; de Meijere, A. Many Density Functional Theory approaches fail to give Reliable Large Hydrocarbon Isomer Energy Differences. *Org. Lett.* **2006**, *8*, 3635−3638.

(46) Frisch, M. J.; Trucks, G. W.; Schlegel, H. B.; Scuseria, G. E.; Robb, M. A.; Cheeseman, J. R.; Scalmani, G.; Barone, V.; Mennucci, B.; Petersson, G. A.; et al. *Gaussian 09*; Gaussian Inc.: Wallingford CT, 2009.

(47) Frisch, E.; Hratchian, H. P.; Dennington, R. D., II; Keith, T. A.; Millam, J.; Nielsen, B.; Holder, A. J.; Hiscocks, J. *GaussView*, version 5.0.8.; Gaussian Inc, 2009.

(48) Boechat, N.; Ferreira, S. B.; Glidewell, C.; Low, J. N.; Skakle, J. M. S.; Wardell, S. M. S. V. 2-Amino-5-trifluoromethyl-1,3,4-thiadiazole and a redetermination of 2-amino-1,3,4-thiadiazole, both at 120 K: chains of edge-fusedR22(8) andR44(10) rings, and sheets ofR22(8) andR66(20) rings. *Acta Crystallogr., Sect. C: Cryst. Struct. Commun.* **2006**, *62*, o42−o44.

(49) Foresman, J. B.; Frisch, A. *Exploring Chemistry with Electronic Structure Methods* 2nd ed.; Gaussian Inc.: Pittsburgh PA, 1996.

(50) Al-Tamimi, A.-M. S.; El-Emam, A. A.; Al-Deeb, O. A.; Prasad, O.; Pathak, S. K.; Srivastava, R.; Sinha, L. Structural and spectroscopic characterization of a novel potential anti-inflammatory agent 3-(adamantan-1-yl)-4-ethyl-1H-1,2,4-triazole-5(4H)thione by first prin-ciple calculations. *Spectrochim. Acta, Part A* **2014**, *124*, 108−123.

(51) Sundaraganesan, N.; Ilakiamani, S.; Saleem, H.; Wojciechowski, P. M.; Michalska, D. FT-Raman and FT-IR spectra, vibrational assignments and density functional studies of 5-bromo-2-nitro-pyridine. *Spectrochim. Acta, Part A* **2005**, *61*, 2995−3001.

(52) Singh, I.; El-Emam, A. A.; Pathak, S. K.; Srivastava, R.; Shukla, V. K.; Prasad, O.; Sinha, L. Experimental and theoretical DFT (B3LYP, X3LYP, CAM-B3LYP and M06-2X) study on electronic structure, spectral features, hydrogen bonding and solvent effects of 4-methylthiadiazole-5-carboxylic acid. *Mol. Simulat.* **2019**, *45*, 1029−1043.

(53) Rao, P. K.; Singh, H. J. Kinetics and mechanism of gas-phase reaction of CF3OCH2CH3 (HFE-263) with the OH radical - a theoretical study. *Can. J. Chem.* **2015**, *93*, 303−310.

(54) Sundius, T. A new damped least-squares method for the calculation of molecular force fields. *J. Mol. Spectrosc.* **1980**, *82*, 138−151.

(55) Sundius, T. Molvib—A flexible program for force field calculations. *J. Mol. Struct.* **1990**, *218*, 321−326.

(56) Sundius, T. Scaling of ab initio force fields by MOLVIB. *Vib. Spectrosc.* **2002**, *29*, 89−95.

(57) Glendening, E. D.; Landis, C. R.; Weinhold, F. Natural bond orbital methods. *Wiley Interdiscip. Rev.: Comput. Mol. Sci.* **2011**, *2*, 1−42.

(58) Keresztury, G.; Holly, S.; Besenyei, G.; Varga, J.; Wang, A.; Durig, J. R. Vibrational spectra of monothiocarbamates-II. IR and Raman spectra, vibrational assignment, conformational analysis and ab initio calculations of S-methyl-N,N-dimethylthiocarbamate. *Spectrochim. Acta, Part A* **1993**, *49*, 2007−2026.

(59) *Handbook of Vibrational Spectroscopy*; Keresztury, G., Chalmers, J. M., Griffith, P. R., Eds.; John Wiley & Sons: New York, 2002; pp 71−87.

(60) Trott, O.; Olson, A. J. AutoDock Vina: Improving the speed and accuracy of docking with a new scoring function, efficient optimization, and multithreading. *J. Comput. Chem.* **2010**, *31*, 455−461.

(61) Morris, G. M.; Goodsell, D. S.; Halliday, R. S.; Huey, R.; Hart, W. E.; Belew, R. K.; Olson, A. J. Automated docking using a Lamarckian genetic algorithm and an empirical binding free energy function. *J. Comput. Chem.* **1998**, *19*, 1639−1662.

(62) Accelrys Software. *Discovery Studio Modeling Environment*. Release 4.0; Accelrys Software: San Diego Calif USA, 2013.

(63) Pettersen, E. F.; Goddard, T. D.; Huang, C. C.; Couch, G. S.; Greenblatt, D. M.; Meng, E. C.; Ferrin, T. E. UCSF Chimera?A visualization system for exploratory research and analysis. *J. Comput. Chem.* **2004**, *25*, 1605−1612.

(64) Fleming, I. *Molecular Orbitals and Organic Chemical Reactions*; John Wiley & Sons: New York, 1976.

(65) Parr, R. G.; Pearson, R. G. Absolute hardness: companion parameter to absolute electronegativity. *J. Am. Chem. Soc.* **1983**, *105*, 7512−7516.

(66) Parr, R. G.; Yang, W. *Functional Theory of Atoms and Molecules*; Oxford University Press: New York, 1989.

(67) Domingo, L. R.; Aurell, M. J.; Pérez, P.; Contreras, R. Quantitative characterization of the global electrophilicity power of common diene/dienophile pairs in Diels-Alder reactions. *Tetrahedron* **2002**, *58*, 4417−4423.

(68) Schneider, G. *Madame Curie Bioscience Database*; Prediction of Drug-Like Properties, 2000.

(69) Glendening, E. D.; Badenhoop, J. K.; Reed, A. E.; Carpenter, J. E.; Bohmann, J. A.; Morales, C. M.; Weinhold, F. *NBO 5.0: Natural Bond Orbital Analysis program*; Theoretical Chemistry Institute, University of Wisconsin: Madison WI, 2001.

(70) Espinosa, E.; Molins, E.; Lecomte, C. Hydrogen bond strengths revealed by topological analyses of experimentally observed electron densities. *Chem. Phys. Lett.* **1998**, *285*, 170−173.

(71) Varsanyi, G. *Vibrational Spectra of Benzene Derivatives*; Academic Press: New York, 1969.

(72) Swaminathan, J.; Ramalingam, M.; Sundaraganesan, N. Molecular structure and vibrational spectra of 3-amino-5-hydroxypyrazole by density functional method. *Spectrochim. Acta, Part A* **2009**, *71*, 1776−1782.

(73) Shukla, V. K.; Sachan, A. K.; Pathak, S. K.; Srivastava, R.; Prasad, O.; Sinha, L. Prediction of molecular properties and spectroscopic profile of Riluzole with different functionals (B3LYP, M06-2X, MPWLYP): A combined theoretical and experimental study. *J. Mol. Struct.* **2016**, *1106*, 265−276.

(74) Pathak, S. K.; Srivastava, R.; Sachan, A. K.; Prasad, O.; Sinha, L. A Combined theoretical and experimental study of conformational and spectroscopic profile of 2-acetamido-5-aminopyridine. *Spectrochim. Acta, Part A* **2015**, *143*, 147−157.

(75) Wojciechowski, P. M.; Zierkiewicz, W.; Michalska, D.; Hobza, P. Electronic structures, vibrational spectra, and revised assignment of aniline and its radical cation: Theoretical study. *J. Chem. Phys.* **2003**, *118*, 10900−10911.

(76) Singh, J. S. Laser Raman and infra-red spectra of biomolecule: 5-aminouracil. *Pranama-J. Phys.* **2008**, *70*, 479−486.

(77) Xavier, R. J.; Dinesh, P. Conformational stability, vibrational spectra, HOMO-LUMO and NBO analysis of 1,3,4-thiadiazolidine-2,5-dithione with experimental (FT-IR and FT-Raman) techniques and scaled quantum mechanical calculations. *Spectrochim. Acta, Part A* **2013**, *113*, 171−181.

(78) Roeges, N. P. C. *A Guide to the Complete Interpretation of Infrared Spectra of Organic Structures*; Wiley: New York, 1994.

(79) Atalay, Y.; Yakuphanoglu, F.; Sekerci, M.; Avcı, D.; Başoğlu, A. Theoretical studies of molecular structure and vibrational spectra of 2-amino-5-phenyl-1,3,4-thiadiazole. *Spectrochim. Acta, Part A* **2006**, *64*, 68−72.

(80) Shukla, V. K.; Al-Alshaikh, M. A.; El-Emam, A. A.; Sachan, A. K.; Srivastava, R.; Prasad, O.; Sinha, L. Conformational search, spectral analysis and electronic properties of 5-(4-Pyridinyl)-1,3,4-thiadiazol-2-amine. *J. Mol. Struct.* **2016**, *1108*, 112−125.

(81) Bezerra, A. C. S.; De Sa, E. L.; Nart, F. C. In Situ Vibrational Study of the Initial Steps during Urea Electrochemical Oxidation. *J. Phys. Chem. B* **1997**, *101*, 6443−6449.

(82) Crane, L. G.; Wang, D.; Sears, L. M.; Heyns, B.; Carron, K. SERS Surfaces Modified with a 4-(2-Pyridylazo)resorcinol Disulfide Derivative: Detection of Copper, Lead, and Cadmium. *Anal. Chem.* **1995**, *67*, 360−364.

(83) Gautam, P.; Prakash, O.; Dani, R. K.; Singh, N. K.; Singh, R. K. Vibrational and quantum chemical investigation of cyclization of thiosemicarbazide group in 1-benzoyl-4-phenyl-3-thiosemicarbazide. *Spectrochim. Acta, Part A* **2014**, *132*, 278−287.

(84) Gunasekaran, S.; Seshadri, S.; Muthu, S. Vibrational spectra and normal coordinate analysis of flucytosine. *Indian J. Pure Appl. Phys.* **2006**, *44*, 581−586.

(85) Singh, N. P.; Yadav, R. A. Vibrational studies of trifluoromethyl benzene derivatives 1 : 2-amino, 5-chloro and 2-amino, 5-bromo benzotrifluorides. *Indian J. Phys. B* **2001**, *75*, 347−355.

(86) Subramanian, M. K.; Anbarasan, P. M.; Manimegalai, S. Molecular structure, vibrational spectroscopic studies and natural bond orbital analysis of 7-amino-4-trifluoromethyl coumarin. *Pranama-J. Phys.* **2010**, *74*, 845−850.

(87) Zhang, R.; Du, B.; Sun, G.; Sun, Y. Experimental and theoretical studies on o-, m- and p-chlorobenzylideneaminoantipyrines. *Spectrochim. Acta, Part A* **2010**, *75*, 1115−1124.

(88) Marchesin, V.; Castro-Castro, A.; Lodillinsky, C.; Castagnino, A.; Cyrta, J.; Bonsang-Kitzis, H.; Fuhrmann, L.; Irondelle, M.; Infante, E.; Montagnac, G.; Reyal, F.; Vincent-Salomon, A.; Chavrier, P. ARF6-JIP3/4 regulate endosomal tubules for MT1-MMP exocytosis in cancer invasion. *J. Cell Biol.* **2015**, *211*, 339−358.

(89) Ren, B.; Wei, X.; Zou, G.; He, J.; Xu, G.; Xu, F.; Huang, Y.; Zhu, H.; Li, Y.; Ma, G.; Yu, P. Cancer testis antigen SPAG9 is a promising marker for the diagnosis and treatment of lung cancer. *Oncol. Rep.* **2016**, *35*, 2599−2605.

(90) Daina, A.; Michielin, O.; Zoete, V. SwissADME: a free web tool to evaluate pharmacokinetics, druglikeness and medicinal chemistry friendliness of small molecules. *Sci. Rep.* **2017**, *7*, 42717.

(91) Lipinski, C. A.; Lombardo, F.; Dominy, B. W.; Feeney, P. J. Experimental and computational approaches to estimate solubility and permeability in drug discovery and development settings 1PII of original article: S0169-409X(96)00423-1. The article was originally published in Advanced Drug Delivery Reviews 23 (1997) 3-25. 1. *Adv. Drug Delivery Rev.* **2001**, *46*, 3−26.

(92) Veber, D. F.; Johnson, S. R.; Cheng, H.-Y.; Smith, B. R.; Ward, K. W.; Kopple, K. D. Molecular Properties That Influence the Oral Bioavailability of Drug Candidates. *J. Med. Chem.* **2002**, *45*, 2615−2623.

(93) Egan, W. J.; Merz, K. M.; Baldwin, J. J. Prediction of Drug Absorption Using Multivariate Statistics. *J. Med. Chem.* **2000**, *43*, 3867−3877.

(94) Mosmann, T. Rapid Colorimetric Assay for Cellular Growth and Survival: Application to Proliferation and Cytotoxicity Assays. *J. Immunol. Methods* **1983**, *65*, 55−63.